International Journal of Heat and Mass Transfer 52 (2009) 3341–3352

Contents lists available at ScienceDirect

International Journal of Heat and Mass Transfer

journal homepage: www.elsevier.com/locate/ijhmt

Critical heat flux for subcooled flow boiling in micro-channel heat sinks

Jaeseon Lee, Issam Mudawar *

Boiling and Two-Phase Flow Laboratory (BTPFL) and Purdue University International Electronic Cooling Alliance (PUIECA), Mechanical Engineering Building, 585 Purdue Mall, West Lafayette, IN 47907-2088, USA

ARTICLE INFO

Article history:
Received 15 February 2008
Received in revised form 17 December 2008
Available online 19 March 2009

Keywords:
Micro-channel
Flow boiling
Critical heat flux
Subcooled boiling

ABSTRACT

Critical heat flux (CHF) was measured and examined with high-speed video for subcooled flow boiling in micro-channel heat sinks using HFE 7100 as working fluid. High subcooling was achieved by pre-cooling the working fluid using a secondary low-temperature refrigeration system. The high subcooling greatly reduced both bubble departure diameter and void fraction, and precluded flow pattern transitions beyond the bubbly regime. CHF was triggered by vapor blanket formation along the micro-channel walls despite the presence of abundant core liquid, which is consistent with the mechanism of Departure from Nucleate Boiling (DNB). CHF increased with increasing mass velocity and/or subcooling and decreasing hydraulic diameter for a given total mass flow rate. A pre-mature type of CHF was caused by vapor back-flow into the heat sink's inlet plenum at low mass velocities and small inlet subcoolings, and was associated with significant fluctuations in inlet and outlet pressure, as well as wall temperature. A systematic technique is developed to modify existing CHF correlations to more accurately account for features unique to micro-channel heat sinks, including rectangular cross-section, three-sided heating, and flow interaction between micro-channels. This technique is shown to be successful at correlating micro-channel heat sink data corresponding to different hydraulic diameters, mass velocities and inlet temperatures.

1. Introduction

1.1. Critical heat flux in subcooled versus saturated flow boiling

Critical heat flux (CHF) is arguably the most important design limit for systems involving heat dissipation from heat-flux controlled surfaces. The occurrence of CHF is associated with a sudden, large reduction in the heat transfer coefficient, which is caused by the loss of liquid contact with the solid surface upon which evaporation or flow boiling is occurring. Depending on heat flux magnitude, thermophysical properties, and operating conditions, the loss of coolant contact can result in surface overheating, burnout, or some other form of catastrophic system failure; hence the importance designers place on accurately determining the CHF limit.

Electronics cooling is a rather recent application where CHF determination is crucial to the safe design and operation of high performance microprocessors. The transition from air-cooling to single-phase liquid cooling and, ultimately, two-phase cooling has been spurred by an unprecedented rise in chip heat flux, brought about by aggressive integration of an increasing number of electronic components in a single chip. Nowhere is this rise more alarming than in defense electronics, such as those found in directed energy laser and microwave weapons, and in radars. Current developments in these applications point to the need to dissipate as high as 1000 W/cm^2 at the device level [1]. This task is complicated by the fact that only dielectric coolants are permitted in these applications. Despite their many attractive attributes, such as high dielectric strength and compatibility with most materials comprising an electronic package, these coolants possess relatively poor thermal transport properties. Therefore, every effort must be made to enhance their cooling potential in order to safely dissipate the anticipated high heat fluxes.

Recently, the authors suggested a thermal management solution for high-flux defense electronics in which the dielectric coolant HFE 7100 is pre-cooled by a secondary refrigeration cooling system before entering a micro-channel heat sink to which the electronic device is attached [2,3]. The refrigeration system provides two key benefits. First, it reduces the temperature of the HFE 7100, which helps maintain relatively low device temperatures when dissipating very high heat fluxes. Second, the low temperature of HFE 7100 helps maintain subcooled flow boiling conditions inside the heat sink, which greatly increases CHF for a given flow rate. This system was capable of dissipating in excess of 700 W/cm^2.

The present study concerns the determination of CHF for this indirect-refrigeration-cooled micro-channel configuration. Unlike most published two-phase micro-channel studies, which involve saturated boiling, the present cooling configuration involves highly

* Corresponding author. Tel.: +1 765 494 5705; fax: +1 765 494 0539.
E-mail address: mudawar@ecn.purdue.edu (I. Mudawar).

0017-9310/$ - see front matter © 2009 Elsevier Ltd. All rights reserved.
doi:10.1016/j.ijheatmasstransfer.2008.12.019

Nomenclature

A_{ch}	cross-sectional area of micro-channel
AR	aspect ratio of micro-channel, H_{ch}/W_{ch}
Bo	boiling number
C_1–C_5	correlation constants
C_D	drag coefficient
CHF	critical heat flux
Co	confinement number
D_b	bubble departure diameter
D_{eq}	equivalent hydraulic diameter for uniformly heated channel
D_h	hydraulic diameter of micro-channel
$D_{h,e}$	hydraulic diameter of micro-channel based on heating perimeter
D_{tran}	diameter corresponding to transition from macro- to micro-behavior
DNB	departure from Nucleated Boiling
G	mass velocity
g	gravitational acceleration
h	enthalpy; heat transfer coefficient
H_{ch}	micro-channel height
h_{fg}	latent heat of vaporization
H_{tc}	distance between thermocouple and bottom wall of micro-channel
k	thermal conductivity
L	length of micro-channel
MAE	mean absolute error
$\dot{m}$	total coolant mass flow rate of micro-channel heat sink
N	number of micro-channels in test section
P	pressure
$PM\text{-}CHF$	pre-mature critical heat flux
q''_c	critical heat flux for uniformly heated circular channel
q''_{eff}	heat flux based on total base area of micro-channel heat sink
$q''_{eff,c}$	critical heat flux based on total base area of micro-channel heat sink
q''_p	heat flux based on micro-channel's three-sided heated perimeter
$q''_{p,c}$	critical heat flux based on micro-channel's three-sided heated perimeter
Re	Reynolds number
T	temperature
T_{tc}	measured copper block temperature
$\bar{T}_w$	bottom wall temperature halfway along micro-channel
TS	test section
U	liquid velocity
W_{ch}	width of micro-channel
W_w	width of copper wall separating micro-channels
We	Weber number
x_e	thermodynamic equilibrium quality, $(h-h_f)/h_{fg}$
$x^*_{e,in}$	pseudo-inlet thermodynamic equilibrium quality with properties based on outlet pressure, $(h_{in}-h_{f,o})/h_{fg,o}$
x_o	outlet thermodynamic equilibrium quality, $(h_o-h_{f,o})/h_{fg,o}$

Greek symbols

β	channel aspect ratio, $\beta < 1$
μ	dynamic viscosity
ρ	density
σ	surface tension

Subscripts

c	critical heat flux
ch	micro-channel
f	saturated liquid
g	saturated vapor
in	test section inlet
MC	micro-channel
o	test section outlet
sat	saturated
sub	subcooled
tc	thermocouple
$tran$	transition from macro- to micro-channel flow
w	bottom wall of micro-channel.

subcooled flow boiling. The key difference between subcooled boiling and saturated boiling is that subcooled boiling occurs at the surface with a bulk liquid temperature below the saturated temperature. With high subcooling, boiling commences when the applied heat flux is capable of superheating liquid adjacent to the surface. Because subcooling is highest in the inlet region of the micro-channel, bubbles near the inlet quickly re-condense at the wall. As the bulk liquid temperature increases along the micro-channel, bubbles are able to grow larger and detach from the surface, mixing into the bulk flow where they undergo partial or full condensation. Condensation greatly reduces the magnitude of void fraction in subcooled compared to saturated boiling. Unlike the drastic flow pattern transitions in saturated flow (bubbly, churn, slug, annular), subcooled flow boiling is dominated by bubbly flow alone. Those differences in flow pattern have a strong bearing on both the mechanism and magnitude of CHF for subcooled versus saturated boiling.

Fig. 1 illustrates these differences in CHF mechanism. For saturated flow boiling, large increases in void fraction trigger a succession of flow regimes. The flow eventually culminates in the high void fraction annular flow pattern, where cooling is sustained by evaporation of a thin liquid film along the surface. CHF results from dryout of the liquid film as the surface is exposed directly to the vapor. While the ensuing downstream mist flow provides some cooling by droplet impact with surface, the heat transfer coefficient is drastically smaller than upstream of the dryout point. Dryout typically occurs with low inlet subcoolings, low mass velocities, and large length-to-diameter ratios, and CHF magnitude with dryout is relatively small.

With highly subcooled flow boiling, bubbly flow persists over much of the channel length, and CHF ensues when bubbles near the wall coalesce into a localized vapor blanket that causes a sharp reduction in the local heat transfer coefficient. This form of CHF is termed Departure from Nucleate Boiling (DNB) and occurs with high inlet subcoolings, high mass velocities, and small length-to-diameter ratios. The magnitude of CHF is much higher than with dryout, and the ensuing surface temperature rise is far more catastrophic.

A significant body of literature has been published that addresses subcooled flow-boiling CHF. The majority of these studies are devoted to the development of correlations from large CHF database or limited experimental data [4–11]; most of these studies are focused on water data and nuclear reactor cooling. Theoretical treatments of DNB are far more limited (e.g., Refs. [12–14]).

Because most prior subcooled boiling studies concern nuclear reactor cooling, available correlations typically address high-pressure water conditions. No effort has yet been made to assess the suitability of these correlations to electronic cooling applications and dielectric coolants.

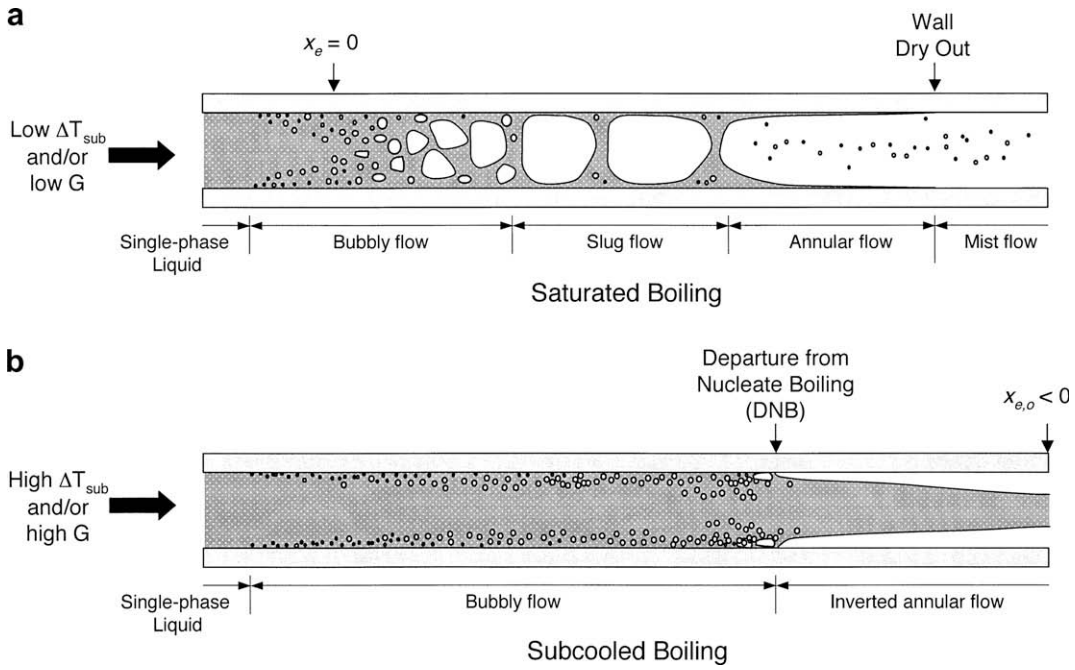

Fig. 1. CHF mechanisms for flow boiling in uniformly heated channel: (a) dryout in saturated flow boiling and (b) DNB in subcooled flow boiling.

1.2. Micro-Channel versus Macro-Channel Flow Boiling

Another limitation of prior flow boiling CHF correlations is that they are derived from data for macro-channel. Despite the intense recent interest in micro-channel heat sinks for electronic cooling applications, very few studies have been published that address CHF determination [15,16]; alas, these studies concern only saturated flow boiling CHF.

Different recommendations have been made concerning the channel size below which the channel begins to behave as a micro-channel. For the most part, recommendations have been based on hydraulic diameter. For example, Thome suggested diameters of 100–600 μm be classified as micro-channels [17].

Distinguishing between macro- and micro-channel flows cannot be based on channel size alone. As will be shown below, a channel may behave as a micro-channel for certain fluids and operating conditions and as a macro-channel for others. Clearly a more rigorous treatment is necessary to define a mechanistically based boundary between the two flow extremes.

For two-phase flow, this boundary is closely related to the ratio of bubble size to channel diameter, the larger the ratio, the more likely that the flow will behave as a micro-channel flow. Kew and Cornwell [18] used this rationale to determine the boundary between micro-channel and macro-channel flows based on a Confinement number defined as

$$Co = \left[\frac{\sigma}{g(\rho_f - \rho_g)D_h^2}\right]^{1/2}. \quad (1)$$

They showed that channels become too confining when $Co > 0.5$, which is where macro-channel assumptions begin to fall apart. Table 1 summarizes hydraulic diameter values corresponding to $Co = 0.5$ for several fluids. Notice that low surface tension fluids, such the dielectric coolants FC-72 and HFE 7100, and refrigerant R134a, have lower hydraulic diameters corresponding to the transition from macro- to micro-channel flow, whereas water, with its higher surface tension, produces micro-channel flow in larger channels. However, the boundary values listed in Table 1 are quite larger than those deemed typical of micro-channel flows.

A key weakness of Eq. 1 is that it is based on the ratio of surface tension force to buoyancy, evidenced by the appearance of gravitational acceleration in the definition of the Confinement number. While this criterion is a good representation for pool boiling in, say, a confined vertical channel, it is not able to account for bubble size in a flow-boiling situation. Aside from surface tension, bubble size in flow boiling is dominated by liquid drag rather than buoyancy. In the present study, an alternative measure of the boundary between macro- and micro-channel flows is developed which incorporates the influence of liquid drag on bubble size. Equating the drag force on the bubble to the surface tension force that holds the bubble to the wall gives

$$C_D\left(\frac{\pi D_b^2}{4}\right)\frac{1}{2}\rho_f U^2 \sim \pi D_b \sigma. \quad (2)$$

A channel tends to confine the flow when the diameter determined from Eq. 2 approaches the diameter of the channel. Therefore, the

Table 1
Fluid properties and hydraulic diameters corresponding to transition from macro- to micro-channel flow for different coolants at one bar based on Eq. 1.

Fluids	T_{sat} [°C]	h_{fg} [kJ/kg]	ρ_f [kg/m^3]	ρ_g [kg/m^3]	σ [mN/m]	Co (D_h = 1.0 mm)	D_{tran} (Co = 0.5) [mm]
Water	99.6	2258	959	0.59	59.0	2.50	5.0
FC-72	55.9	83.54	1603	13.1	12.0	0.88	1.75
R134a	−26.4	217.2	1378	5.19	15.5	1.07	2.14
HFE 7100	59.6	111.7	1373	9.58	15.7	1.08	2.17

channel diameter corresponding to the transition from macro- to micro-channel flow can be determined from the relation

$$D_{tran} \le D_b. \tag{3}$$

For circular channels, D_{tran} is simply the diameter of the channel.

Two-phase micro-channel flow applications of practical interest are characterized by modest laminar Reynolds numbers, generally greater than 50. Under these conditions, the drag coefficient can be determined from [19]

$$C_D = \frac{24}{Re_{tran}}\left(1 + \frac{3}{160}Re_{tran}\right). \tag{4}$$

Combining Eqs. (2)–(4) and substituting $G = \rho_f U$, yield the following criterion for the transitional channel dimension,

$$D_{tran} = \frac{160}{9}\frac{(\sigma\rho_f - 3\mu_f G)}{G^2}. \tag{5}$$

Table 2 shows calculated values of D_{tran} for water and HFE 7100 based on Eq. 5. Notice how these values are significantly smaller than those given in Table 1, and more representative of values deemed typical of micro-channel flow in recent experimental studies. Table 2 also shows decreasing surface tension and/or increasing mass velocity enables smaller channels to behave as macro-channels.

It is interesting to note that Eq. 5 can also be expressed as a Weber number criterion for confinement

$$We_{tran} = \frac{160}{9}\frac{1}{\left(1 + \frac{160}{3Re_{tran}}\right)}, \tag{6}$$

which can be approximated as

$$We_{tran} = \frac{160}{9} \tag{7}$$

for high mass velocities. Eq. 7 shows Weber number plays an important role in micro-channel flows, and its effect must therefore be incorporated in any micro-channel CHF correlation. This important issue will be discussed later in this paper.

2. Experimental methods

2.1. Test facility and micro-channel test sections

Fig. 2 shows a schematic diagram of the flow control system used in the present CHF experiments. The system consists of a primary HFE 7100 loop that contains the micro-channel test module, and a secondary vapor compression refrigeration system. The primary coolant is subcooled by rejecting heat to the refrigeration system via an intermediate heat exchanger.

HFE 7100 is an environmentally friendly non-ozone-depleting dielectric fluid with very low global warming potential. Because of its inertness and high dielectric strength, it is ideally suited for electronic cooling applications. Its freezing point is below −100 °C, which renders it very suitable for low-temperature cooling situations.

As shown in Fig. 3(a) and (b), the test module consists of a copper block, a G-11 plastic housing, a transparent cover, four cartridge heaters, and a bottom support plate. Using thin carbide cutters, the micro-channels were machined into the top 10-mm long and 5-mm wide test surface of the copper block. Four different micro-channel test sections were tested; Table 3 provides key dimensions of the micro-channels in each test section.

The plastic housing provides inlet and outlet plenums for the micro-channels, Fig. 3(c), in addition to access ports for temperature and pressure measurements. Heat is supplied to the test surface from the four cartridge heaters that are inserted into bores in the underside of the copper block.

While four different micro-channel geometries were tested, because of system limitations, the majority of CHF data were obtained with the two larger hydraulic diameter test sections. For a given flow rate, the two smaller hydraulic diameters produced much larger mass velocities, pressure drops, and CHF values than the two larger diameters. To prevent any damage to the module parts due to overheating, testing was terminated at $q''_{eff} = 700\ \mathrm{W/cm^2}$. This limit precluded the attainment of CHF data for the two smaller diameter test sections.

2.2. Operating conditions and measurements

The temperature of the primary coolant (HFE 7100) at the inlet to the micro-channel test section was finely adjusted using an automatic feedback control feature in the refrigeration system. The system provided inlet temperatures in the range of −30 to 20 °C. Aside from inlet temperature, the test matrix for the present study included variations of flow rate of the primary coolant and heat flux; a constant test section's outlet pressure of 1.138 bar was maintained throughout the study.

Test were performed by increasing electric power input to the cartridge heaters in small increments, and were terminated at CHF, which was easily detected by a sudden unsteady rise in the copper block's temperature. CHF was determined as the average of the last steady-state heat flux value before CHF and the next heat flux that initiated CHF.

The test module's instrumentation includes pressure transducers and thermocouples for both the inlet and outlet plenums. Type-T thermocouples are inserted in the copper block beneath the micro-channels to measure the copper block's temperatures. Other measurements include electrical power input to the test section's four cartridge heaters using a Wattmeter, and mass flow rate using the Coriolis flow meter. All measurements were made simultaneously and processed by an HP3852 data acquisition system.

To determine q''_{eff}, power measurements were corrected for heat loss as discussed in Ref. [2]. Uncertainties in the temperature measurements were ±0.5 °C for inlet fluid temperature control and ±0.3 °C for all the thermocouple readings. Accuracies of the other measurement instruments were as follows: ±0.5% for the pressure transducers, ±0.1% for the Coriolis flow meter, and ±0.1% for the Wattmeter.

Table 2
Fluid properties and hydraulic diameters corresponding to transition from macro- to micro-channel flow for water and HFE 7100 at one bar based on Eq. 5.

Fluids	T_{sat} [°C]	ρ_f [kg/m3]	μ_f [kg/m.s]	σ [mN/m]	G [kg/m^{2}s]	D_{tran} [mm]
Water	99.6	959	2.83×10^{-4}	59.0	500	3.99
					1000	0.990
					2000	0.243
HFE 7100	59.6	1373	3.57×10^{-4}	15.7	500	1.49
					1000	0.364
					2000	0.0863

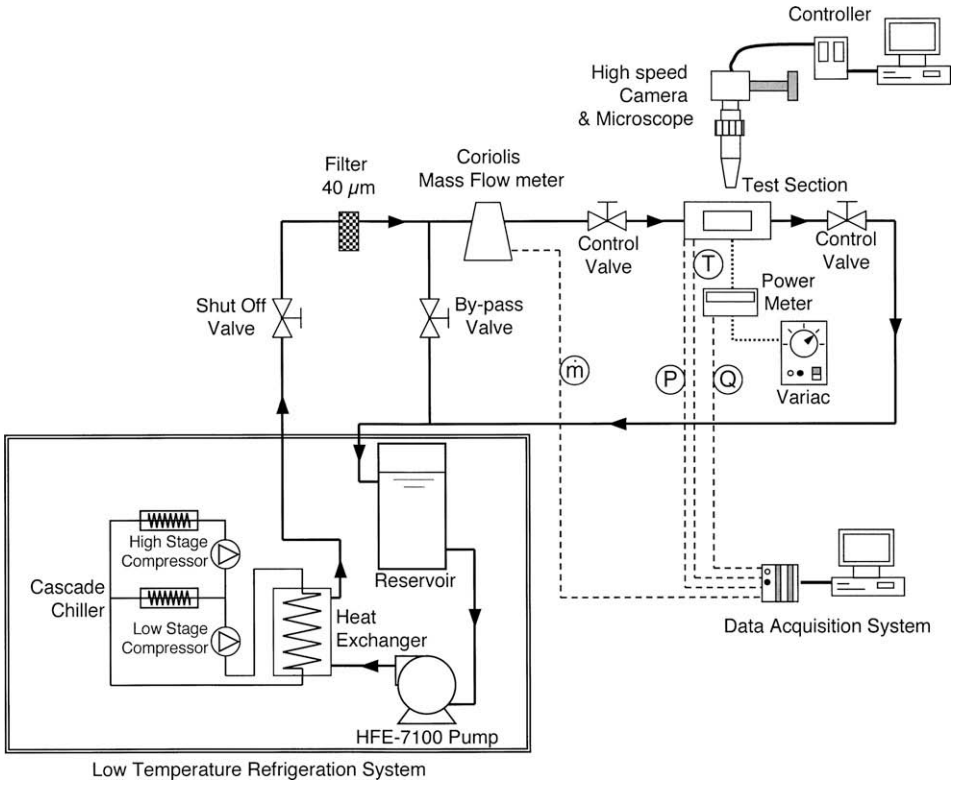

Fig. 2. Flow diagram for indirect refrigeration cooling system.

Table 3
Test section dimensions.

	W_{ch} [μm]	W_w [μm]	H_{ch} [μm]	AR	D_h [μm]	L [cm]	N
TS#1	123.4	84.2	304.9	2.47	175.7	1.0	24
TS#2	123.4	84.6	526.9	4.27	200.0	1.0	24
TS#3	235.2	230.3	576.8	2.45	334.1	1.0	11
TS#4	259.9	205.0	1041.3	4.01	415.9	1.0	11

3. Experiment results and discussion

3.1. CHF trends and flow visualization results

Several key parameters were used to characterize flow conditions and CHF. Aside from total flow rate, $\dot{m}$, of the primary coolant, tests were also based on mass velocity, which is defined as

$$G = \frac{\dot{m}}{NA_{ch}}, \tag{8}$$

where N is the number of micro-channels in the heat sink, and A_{ch} the cross-sectional area of each micro-channel. Two definitions are used for heat flux as shown in Fig. 4. The first is the effective heat flux, q''_{eff}, which is based on the total base area of the micro-channel heat sink. This would be equivalent to the heat flux dissipated from an electronic device to which the micro-channel heat sink is attached. The second, q''_p, is the average heat flux along the three thermally conducting walls of the rectangular micro-channel. This latter definition is used to compare present CHF values to those determined from prior CHF correlations, which are typically derived from databases for uniformly heated channels. As illustrated in Fig. 4, q''_p is related to q''_{eff} by the relation

$$q''_p = \frac{q''_{eff}(W_{ch} + W_w)}{(W_{ch} + 2H_{ch})}. \tag{9}$$

Fig. 5 shows representative flow boiling curves for two different micro-channel test sections and two mass flow rates. The micro-channel's mean base temperature, $\bar{T}_w$, halfway along the micro-channel was determined with a simple fin model and the assumption of 1-D conduction using the unit cell shown in Fig. 4. Details of the procedure used to determine $\bar{T}_w$ is provided in a previous study by the authors [2]. Fig. 5 shows increasing the flow rate increases CHF for both test sections. Furthermore, the micro-channel with the smaller hydraulic diameter yields higher CHF values. This can be explained by the smaller micro-channel's greater mass velocity for the same mass flow rate as the larger micro-channel. However, this trend is by no means conclusive or monotonic. For example, comparing the data in Fig. 5 for TS#3 at G = 1,341 kg/m^2.s with data for TS#4 at G = 1,007 kg/m^2.s shows the smaller G yielding a higher CHF value. A more effective way to assess the influence of G on CHF is to use q''_p rather than q''_{eff}. For the G = 1,341 kg/m^2.s case, $q''_{eff} = 325.8$W/cm^2 but $q''_p = 109.2$W/cm^2, whereas $q''_{eff} = 417.0$W/cm^2 and $q''_p = 82.8$W/cm^2 for the G = 1,007 kg/m^2.s case. This shows using q''_p does yield the expected trend of increasing CHF with increasing G and is therefore a more effective parameter for correlating micro-channel CHF data. Unfortunately, further verification of the benefits of smaller micro-channels was not possible for all micro-channel sizes, given the lack of CHF data for test sections TS#1 and TS#2. However, prior work by the authors has shown very small diameters promote early transition from bubbly to slug flow, especially in narrow channels [2]. A large increase in void fraction may compromise the magnitude of CHF.

Fig. 5 shows two different types of CHF, three are indicated as 'normal CHF' and one as 'pre-mature CHF' or PM-CHF. Differences between these CHF types can be best explained with the aid of images obtained with high-speed video.

Fig. 6 shows the typical occurrence of 'normal CHF.' Prior to CHF, there is significant near-wall bubble activity, with an abundance of liquid in the core. At CHF, bubbles suddenly coalesce into

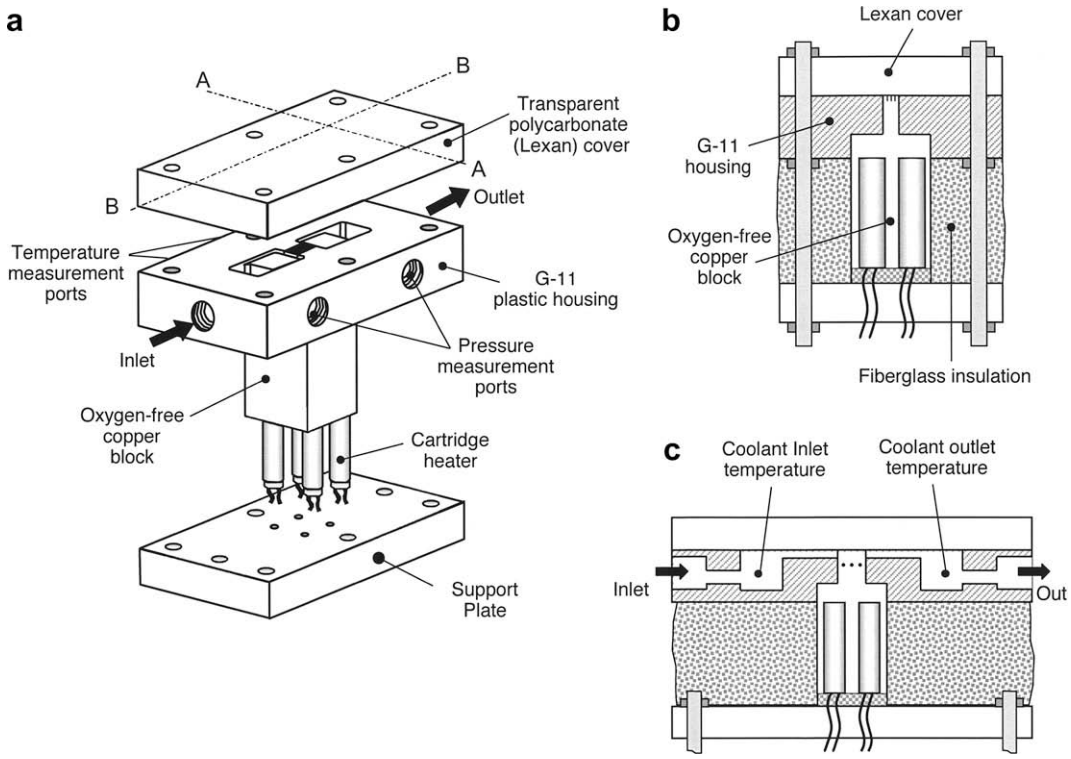

Fig. 3. (a) Isometric view of micro-channel test section. (b) Cross-sectional view (A–A). (c) Side sectional view (B–B).

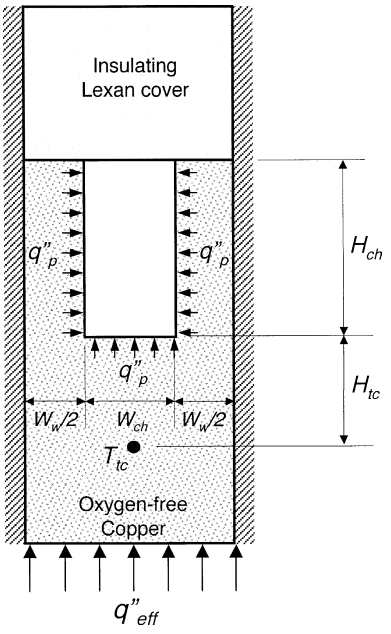

Fig. 4. Micro-channel unit cell.

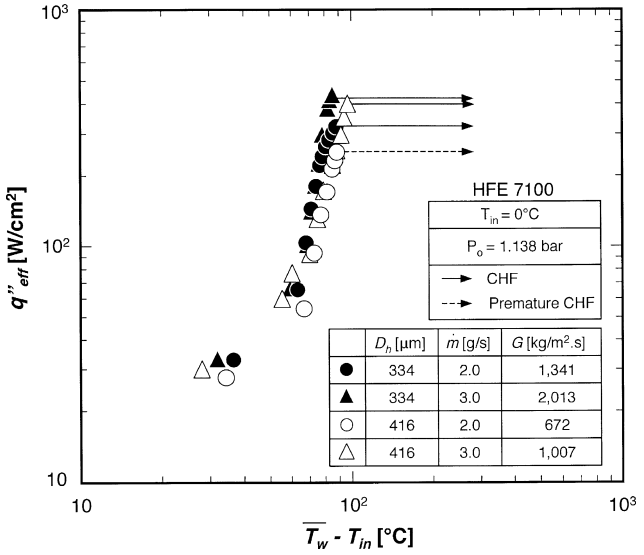

Fig. 5. Boiling curves for subcooled flow boiling conditions.

a continuous vapor blanket, thermally insulating the micro-channel walls from liquid contact. This behavior is consistent with the definition of DNB (see Fig. 1), and is manifest by a sudden sharp rise in the micro-channel's base temperature.

Fig. 7 shows a series of images of the flow during pre-mature CHF. High void fraction appears to momentarily increase pressure drop, preventing liquid from entering the micro-channels. This forces vapor backwards towards the inlet plenum. Vapor begins to accumulate in the inlet plenum as liquid inside the micro-channels is evaporated, causing wall temperature to rise. During the vapor back flow, pressure in the inlet plenum begins to rise until it is capable of resisting the vapor back flow. Fresh liquid is then reintroduced into the micro-channels, re-wetting the micro-channel walls and decreasing the wall temperature as the inlet temperature also decreases. This cycle is repeated several times, with the mean wall temperature increasing between cycles. Eventually, the wall temperature begins to rise more rapidly, signaling the commencement of PM-CHF. Fig. 8 shows transient records of the downstream wall thermocouple, the inlet and outlet pressure transducers and the Coriolis flow meter before and during PM-CHF. Notice the large increase in the amplitude of the temperature and pressure signals as well as the increase in mean wall temperature during PM-CHF.

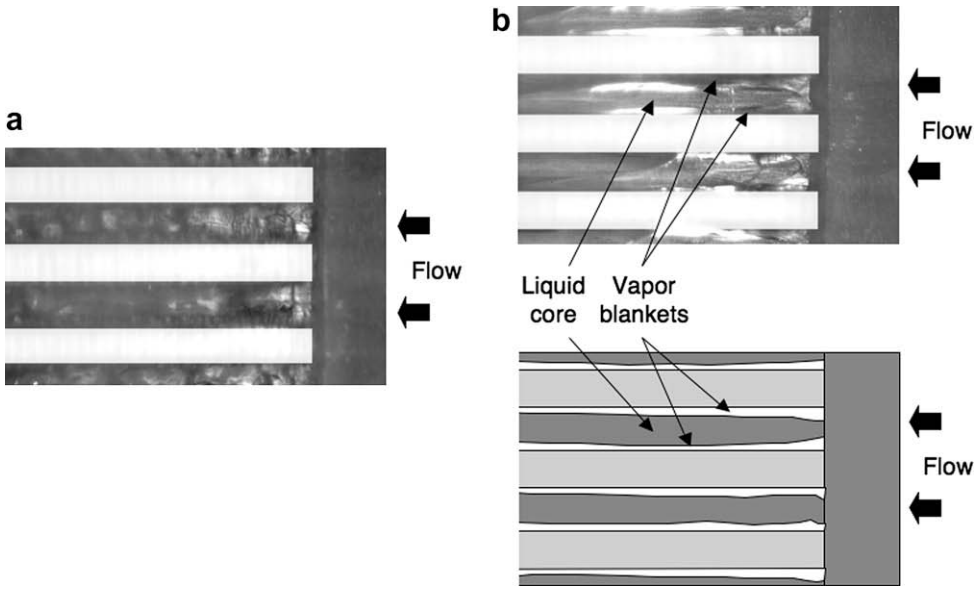

Fig. 6. Flow images for normal DNB with TS#3 (D_h = 334.1 μm) at T_{in} = 0 °C and G = 1341 kg/m^2.s for (a) $q''_{eff} = 318.3$W/cm^2, (b) $q''_{eff} > q''_{eff} = 325.8$W/cm^2.

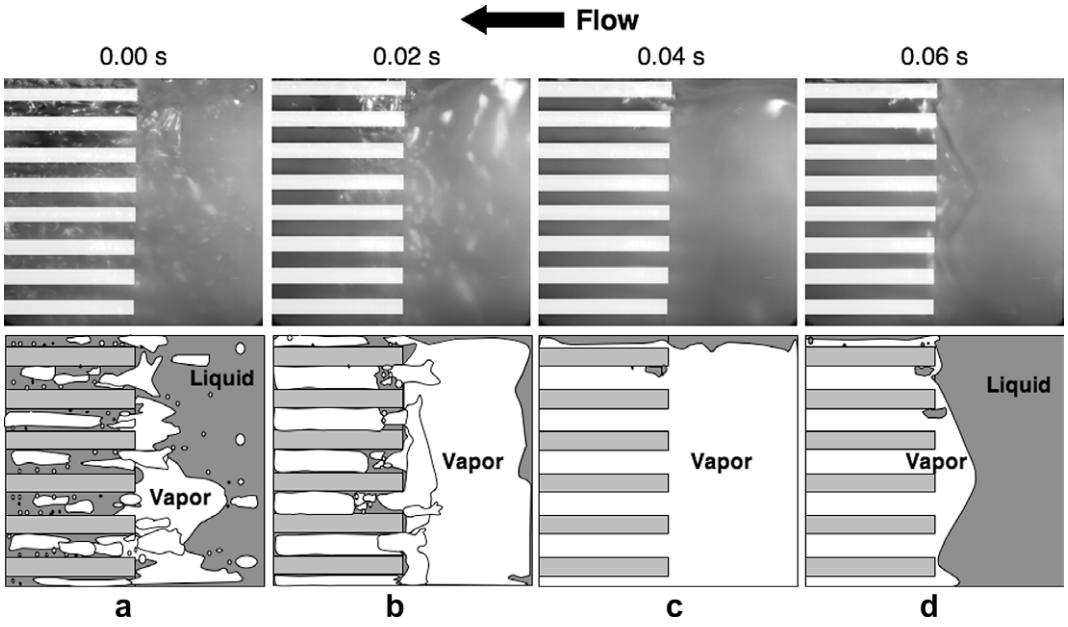

Fig. 7. Pre-mature CHF and flow oscillations in TS#4 (D_h = 415.9 μm) for T_{in} = 0 °C, G = 672 kg/m^2 s, and q'' > 250.0 W/cm^2: (a) initial vapor pocket buildup in upstream plenum, (b) growth of vapor mass, (c) complete blockage of inlet plenum by vapor mass, and (d) purging of vapor mass along micro-channels (adapted from Ref. [2]).

Overall, PM-CHF occurs at low mass velocities and low subcoolings [15]. High mass velocities preclude the occurrence of PM-CHF by providing sufficiently large momentum to resist the vapor back flow. High subcooling serves to decrease vapor void fraction through stronger condensation, which greatly reduces the vapor blockage.

Fig. 9 shows the variation of CHF, based on heated perimeter, with inlet subcooling and mass velocity for test sections TS#3 and TS#4, including PM-CHF data. Overall, CHF increases monotonically with increases in inlet subcooling and/or mass velocity. Notice that PM-CHF is encountered mostly at low mass velocities and/or low subcoolings. Special attention is given in this study to distinguishing between normal and PM-CHF data when assessing prior correlations. Table 4 provides all the CHF data measured in the present study. The database consists of 45 data points of which 13 are PM-CHF.

3.2. New CHF correlation

CHF correlations are based on either inlet (upstream) channel conditions or outlet (local) conditions. Pressure, mass velocity and diameter appear in both types of correlations. However, the effect of inlet quality in inlet conditions correlations is expressed in terms of inlet enthalpy (or inlet subcooling or quality); these correlations also account for quality variations along the channel through their dependence on channel length.

$$q''_c = \mathrm{f}(G, P, h_{in}, D, L). \tag{10}$$

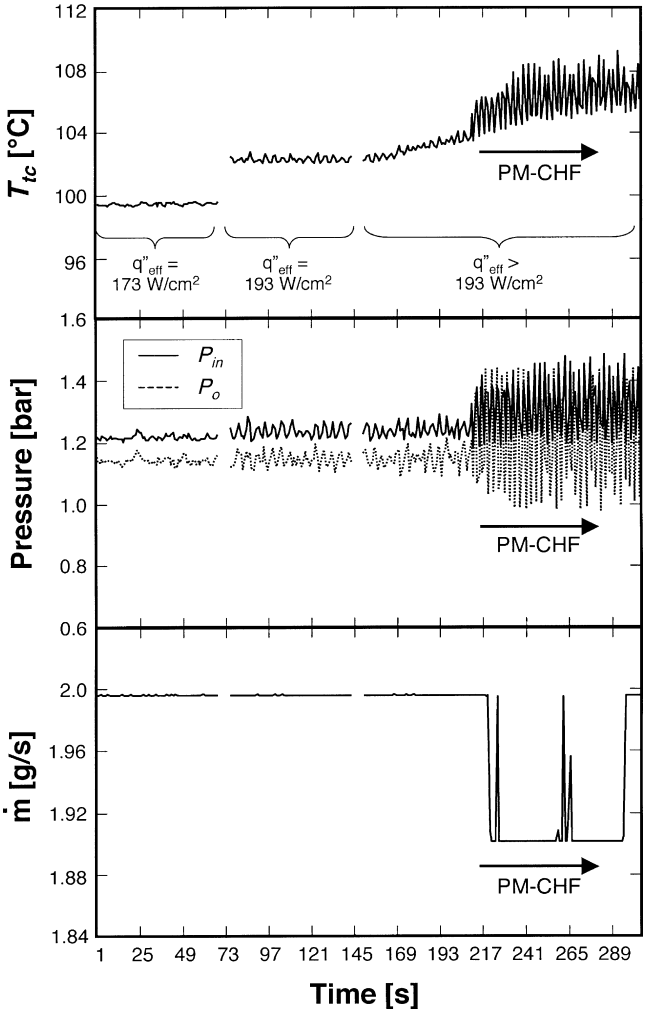

Fig. 8. Variations of temperature, pressure, and mass flow rate associated with premature CHF for TS#4, T_{in} = 20 °C and G = 671 kg/m² s.

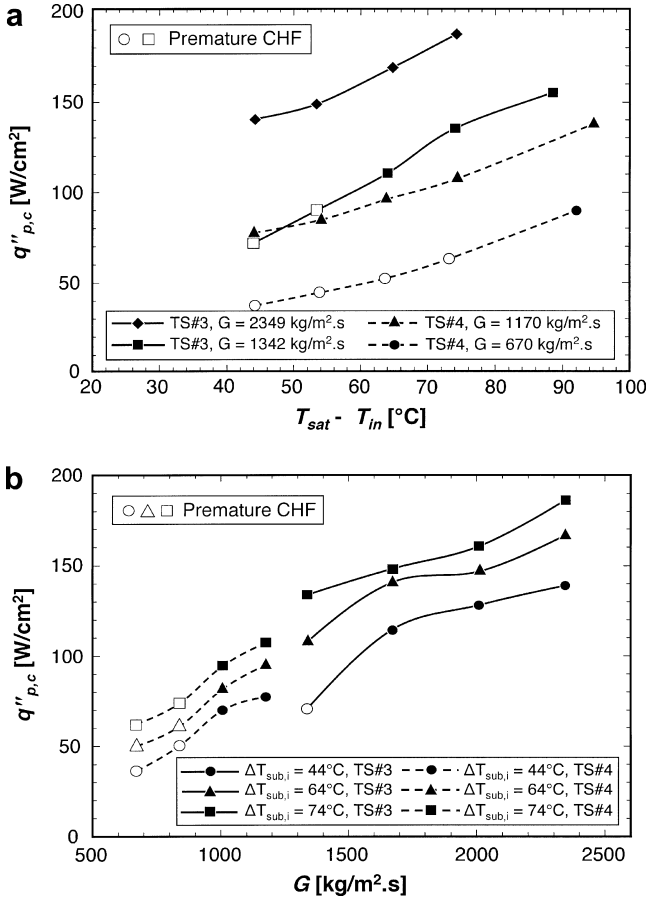

Fig. 9. Variation of subcooled boiling CHF with (a) inlet subcooling and (b) mass velocity.

The parameters in Eq. 10 are independent variables that are readily available for CHF determination. On the other hand, while outlet conditions correlations are also based pressure, mass flux and diameter, they account for the effects of quality through outlet enthalpy (or outlet subcooling or quality) since they are based on the premise that CHF occurs locally at the channel outlet.

$$q''_c = f(G, P, D, h_o). \tag{11}$$

Therefore, use of an outlet conditions correlation involves indirect estimation of CHF since outlet quality must first be calculated with the CHF data point using an energy balance over the entire heated length. This is why channel length does not appear in Eq. 11.

Developing universal CHF correlations that are applicable to broad ranges of operating conditions requires amassing large CHF databases. This goal was accomplished by Hall and Mudawar [6–7] through the Purdue University - Boiling and Two Phase Flow Laboratory (PU-BTPFL) CHF database, which was assembled with 32,544 data points from over 100 sources, of which 5544 data points are subcooled CHF. The primary objectives of their study were to (a) amass all existing water CHF databases for both vertical upflow and horizontal flow in a uniformly heated channel, (b) assess these databases on a point-by-point basis to eliminate any erroneous data, (c) compile all known subcooled CHF correlations for water flow in a uniformly heated tube, (d) evaluate these correlations using the CHF database corrected for the erroneous data, and (e) develop simple, subcooled CHF correlations that are superior in accuracy to existing correlations and look-up tables. Hall and Mudawar recommended two correlations for subcooled (negative outlet quality) flow boiling CHF, one is inlet conditions based and the second outlet conditions. In a separate study, Mudawar et al. [4,5] examined a subset of the PU-BTPFL database that involved ultra-high-flux subcooled flow boiling CHF in small diameter tubes in the range of D = 0.406–2.54 mm with relatively small L/D ratios, and recommended inlet conditions and outlet conditions correlations that are better suited for this subset. This subset includes the worlds highest CHF value of 27,600 W/cm² measured with a uniformly heated channel [4]. Table 5 summarizes the correlations based on the entire PU-BTPFL database and on the small diameter subset. Because of the superiority of these four correlations to other published correlations has already been systematically ascertained [5,7], these correlations are used in the present study as a starting point for developing CHF correlations for micro-channel heat sinks.

The present micro-channel heat sink configuration poses the following challenges when attempting to assess or utilize prior CHF correlations:

(1) *Working fluid:* most published CHF correlations for subcooled flow boiling are derived from water data; the present data were obtained using HFE 7100 as working fluid.

Table 4
Present CHF data.

No.	D_h [μm]	L/D_h	G [kg/m^2 s]	T_{in} [°C]	T_o [°C]	$\Delta T_{sub,in}$ [°C]	$\Delta T_{sub,o}$ [°C]	P_{in} [bar]	P_o [bar]	x_{in}	x_o	$q''_{eff,c}$ [W/cm^2]	$q''_{p,c}$ [W/cm^2]	Notes
1	175.7	56.9	2213.9	0.04	43.82	68.28	19.75	1.3135	1.1339	−0.652	−0.206	301.1	85.3	PM-CHF
2	175.7	56.9	2215.9	−23.60	49.88	95.92	13.88	1.4810	1.1408	−0.888	−0.145	513.8	145.5	
3	200.0	50.0	1276.7	−0.13	42.99	67.46	20.72	1.2742	1.1388	−0.656	−0.216	311.4	55.0	PM-CHF
4	200.0	50.0	1282.1	−22.79	30.34	90.69	33.50	1.2968	1.1435	−0.881	−0.348	435.0	76.8	
5	200.0	50.0	1924.2	−0.30	38.16	69.2	25.66	1.3369	1.1429	−0.659	−0.268	403.5	71.3	PM-CHF
6	334.1	29.9	1338.1	19.62	50.84	46.7	13.04	1.2352	1.1451	−0.459	−0.137	210.9	70.7	PM-CHF
7	334.1	29.9	1338.3	10.14	47.29	56.12	16.45	1.2331	1.1399	−0.553	−0.172	265.6	89.0	PM-CHF
8	334.1	29.9	1341.2	−0.42	49.64	67.21	14.43	1.2534	1.1520	−0.663	−0.151	325.8	109.2	
9	334.1	29.9	1338.2	−10.46	45.15	77.5	18.51	1.2630	1.1373	−0.758	−0.193	399.6	133.9	
10	334.1	29.9	1341.1	−24.92	34.77	91.95	29.02	1.2628	1.1418	−0.901	−0.302	459.1	153.9	
11	334.1	29.9	1672.8	19.30	59.13	49.98	4.94	1.3522	1.1519	−0.464	−0.052	340.6	114.1	
12	334.1	29.9	1673.8	10.02	52.97	58.41	10.82	1.3179	1.1419	−0.555	−0.113	366.0	122.7	
13	334.1	29.9	1673.5	−0.61	47.51	68.96	16.46	1.3145	1.1484	−0.664	−0.172	423.1	141.8	
14	334.1	29.9	1673.5	−10.04	40.42	77.89	23.32	1.2949	1.1402	−0.755	−0.243	441.8	148.1	
15	334.1	29.9	1673.6	−29.66	26.61	97.59	37.18	1.2981	1.1419	−0.947	−0.386	534.4	179.1	
16	334.1	29.9	2009.9	19.29	57.83	51.29	5.96	1.4062	1.1417	−0.461	−0.062	381.7	127.9	
17	334.1	29.9	2006.4	9.73	52.71	59.96	10.99	1.3692	1.1387	−0.557	−0.115	417.7	140.0	
18	334.1	29.9	2013.3	−0.46	43.48	68.7	20.34	1.3102	1.1429	−0.660	−0.212	442.0	148.1	
19	334.1	29.9	2008.5	−9.42	37.56	77.9	26.03	1.3198	1.1345	−0.746	−0.271	479.2	160.6	
20	334.1	29.9	2017.1	−28.77	25.41	96.78	38.39	1.3010	1.1421	−0.938	−0.399	592.3	198.5	
21	334.1	29.9	2345.1	19.39	56.04	52.14	7.68	1.4464	1.1393	−0.459	−0.080	414.4	138.9	
22	334.1	29.9	2344.9	10.20	47.73	60.68	15.95	1.4187	1.1379	−0.552	−0.167	439.6	147.3	
23	334.1	29.9	2345.1	−1.17	42.15	71.32	21.51	1.3880	1.1373	−0.666	−0.225	500.0	167.6	
24	334.1	29.9	2345.5	−10.67	37.02	80.17	26.66	1.3611	1.1379	−0.760	−0.278	555.2	186.1	
25	415.9	24.0	670.5	19.41	45.96	45.2	17.88	1.1716	1.1437	−0.460	−0.187	183.1	36.3	PM-CHF
26	415.9	24.0	670.5	9.75	43.27	54.74	20.39	1.1671	1.1370	−0.556	−0.213	219.0	43.5	PM-CHF
27	415.9	24.0	671.9	−0.07	40.88	64.68	22.84	1.1714	1.1393	−0.655	−0.238	257.1	51.0	PM-CHF
28	415.9	24.0	670.2	−9.62	35.07	74.24	28.59	1.1718	1.1373	−0.749	−0.298	312.2	62.0	PM-CHF
29	415.9	24.0	671.0	−28.48	36.28	93.89	27.67	1.2010	1.1477	−0.937	−0.289	445.7	88.5	
30	415.9	24.0	838.7	19.30	50.52	46.03	13.25	1.1982	1.1412	−0.461	−0.139	253.8	50.4	PM-CHF
31	415.9	24.0	838.6	9.36	42.61	55.7	21.18	1.1881	1.1417	−0.561	−0.221	274.7	54.5	PM-CHF
32	415.9	24.0	838.8	−0.04	37.92	65.17	25.85	1.1908	1.1410	−0.656	−0.269	313.2	62.1	PM-CHF
33	415.9	24.0	838.7	−10.08	33.69	75.17	29.94	1.1892	1.1362	−0.754	−0.312	372.3	73.9	PM-CHF
34	415.9	24.0	838.7	−27.84	35.45	93.44	28.29	1.2081	1.1401	−0.928	−0.295	556.3	110.4	
35	415.9	24.0	1007.0	18.96	57.37	47.63	6.57	1.2457	1.1471	−0.466	−0.069	352.3	69.9	
36	415.9	24.0	1007.0	9.27	53.78	57.17	10.11	1.2399	1.1453	−0.564	−0.106	401.9	79.8	
37	415.9	24.0	1007.0	−0.49	43.37	66.86	20.76	1.2372	1.1542	−0.665	−0.217	417.0	82.8	
38	415.9	24.0	1007.0	−10.88	38.67	76.85	24.87	1.2219	1.1330	−0.760	−0.259	477.1	94.7	
39	415.9	24.0	1009.0	−30.17	24.75	95.55	39.07	1.2001	1.1430	−0.952	−0.406	603.1	119.7	
40	415.9	24.0	1176.0	19.51	56.02	47.68	7.88	1.2690	1.1458	−0.460	−0.083	389.2	77.2	
41	415.9	24.0	1173.0	9.43	49.34	57.33	14.40	1.2524	1.1400	−0.560	−0.151	425.6	84.5	
42	415.9	24.0	1176.0	−0.28	44.16	67.1	19.64	1.2546	1.1423	−0.658	−0.205	483.9	96.0	
43	415.9	24.0	1176.0	−10.82	36.80	77.47	26.82	1.2479	1.1356	−0.761	−0.279	541.6	107.5	
44	415.9	24.0	1176.0	−31.01	31.78	97.57	31.98	1.2447	1.1407	−0.959	−0.333	693.0	137.5	
45	415.9	24.0	1346.0	0.09	47.00	67.28	16.72	1.2757	1.1395	−0.654	−0.175	571.8	113.5	

(2) *Partial circumferential heating:* while the present micro-channels are heated on three sides, prior CHF correlations are typically derived from data for uniform circumferential heating.
(3) *Channel cross-section:* most prior correlations are derived from data for circular channels; the present data involves rectangular channels.
(4) *Multi-channel interactions:* flow interactions between micro-channels can have an appreciable effect on CHF for micro-channel heat sinks. Prior CHF correlations do not account for this effect.
(5) *Small channel size:* with a few exceptions, prior CHF correlations are based on data for macro-channels that are much larger than those of micro-channel heat sinks.
(6) *Pre-mature CHF:* this phenomenon appears to be unique to micro-channel heat sinks and, therefore, cannot be predicted by prior CHF correlations.

The applicability of water-based CHF correlations to other fluids is commonly justified by the broad range of databases upon which a correlation is developed, especially when a correlation is presented in dimensionless form. Partial circumferential heating and the effects of the rectangular geometry in the present micro-channel heat sinks is accounted for by using a hydraulic diameter based on the heated perimeter,

$$D_{h,e} = \frac{4A_{ch}}{P_{h,e}} = \frac{4W_{ch}H_{ch}}{(W_{ch} + 2H_{ch})}, \tag{12}$$

and accounting for the micro-channel's aspect ratio, β, using the following approach.

For a uniformly heated channel, the single-phase convection heat transfer coefficient prevalent in the highly subcooled inlet is given by the relation [20]

$$Nu = \frac{hD_{eq}}{k_f} = 4.36. \tag{13}$$

For a rectangular channel that is heated along three sides, the single-phase convection heat transfer coefficient can be derived from the modified relation [21]

$$Nu_3 = \frac{hD_{h,e}}{k_f} = 8.235f(\beta), \tag{14}$$

where $f(\beta) = 1 - 1.833\beta + 3.767\beta^2 - 5.814\beta^3 + 5.361\beta^4 - 2.0\beta^5$. (15)

Combining Eqs. 13 and 14 provides a relation for equivalent diameter for the present micro-channel configuration.

Table 5
Subcooled boiling CHF correlations.

Author(s) [Ref.]	Remarks	Correlations
Hall & Mudawar [7]	Outlet-conditions based	$Bo_c = \frac{q''_c}{Gh_{fg}} = C_1 We_D^{C_2}\left(\frac{\rho_f}{\rho_g}\right)^{C_\alpha}\left[1 - 1C_4\left(\frac{\rho_f}{\rho_g}\right)_5^C x_0\right]$ $C_1 = 0.0722$, $C_2 = -0.312$, $C_3 = -0.644$, $C_4 = 0.900$, $C_5 = 0.724$
Hall & Mudawar [7]	Inlet-conditions based	$Bo_c = \frac{q''_c}{Gh_{fg}} = \frac{C_1 We_D^{C_2}(\rho_f/\rho_g)\left[1 - C_4(\rho_f/\rho_g)_5^C x^*_{e,in}\right]}{1 + 4C_1C_4 We_D^{C_2}(\rho_f/\rho_g)^{C_3+C_5}(L/D)}$ $C_1 = 0.0722$, $C_2 = -0.312$, $C_3 = -0.644$, $C_4 = 0.900$, $C_5 = 0.724$
Hall & Mudawar [5]	Outlet-conditions based; ultra-high heat flux	$Bo_c = \frac{q''_c}{Gh_{fg}} = C_1 We_D^{C_2}\left(\frac{\rho_f}{\rho_g}\right)\left[1 - C_4\left(\frac{\rho_f}{\rho_g}\right)^{C_5} X_0\right]$ $C_1 = 0.0332$, $C_2 = -0.235$, $C_3 = -0.681$, $C_4 = 0.684$, $C_5 = 0.832$
Hall & Mudawar [5]	Inlet-conditions based; ultra-high heat flux	$Bo_c = \frac{q''_c}{Gh_{fg}} = \frac{C_1 We_D^{C_2}(\rho_f/\rho_g)^{C_3}\left[1 - C_4(\rho_f/\rho_g)_5^C x^*_{e,in}\right]}{1 + 4C_1C_4 We_D^{C_2}(\rho_f/\rho_g)^{C_3+C_5}(L/D)}$ $C_1 = 0.0332$, $C_2 = -0.235$, $C_3 = -0.681$, $C_4 = 0.684$, $C_5 = 0.832$

$$D_{eq} = \frac{D_{h,e}}{1.889 f(\beta)}. \tag{16}$$

This diameter replaces D in all We_D and L/D terms of the CHF correlations given in Table 5.

The CHF correlations for micro-channel heat sinks must account for two additional effects: multi-channel interactions and small channel size. As discussed in the Introduction, these effects are closely associated with bubble confinement, which can be expressed in terms of the Weber number as suggested by Eq. 7. Accounting for the effects of the rectangular geometry and three-sided heating, the Weber number is expressed as

$$We_{D_{eq}} = \frac{G^2 D_{eq}}{\sigma \rho_f}. \tag{17}$$

Therefore, the CHF correlation for the micro-channel heat sink can be obtained by modifying the correlations provided in Table 5 according to the relation

$$Bo_{c,MC} = Bo_c f(We_{D_{eq}}), \tag{18}$$

where $Bo_{c,MC}$ is the Boiling number corresponding to CHF in the micro-channel heat sink and Bo_c is the Boiling number at CHF obtained from the correlations given in Table 5.

This technique for correlating CHF data for micro-channel heat sinks only requires the determination of $f(We_{D_{eq}})$. Using the present database for micro-channel heat sinks, this parameter was fitted as

$$f(We_{D_{eq}}) = We_{D_{eq}}^{0.121}. \tag{19}$$

Both of the inlet conditions correlations given in Table 5 provided good predictions of the present CHF data. However, the ultra-high-heat-flux correlation provided a slightly better MAE of 8.0% compared to 10.7% for the other correlation. Fig. 10 compares the predictions of Eqs. 18 and 19 based on the ultra-high-heat-flux inlet conditions correlation to the experimental micro-channel CHF database, excluding the PM-CHF data. Fig. 10 shows all the data falling within ±20% from the predictions. Fig. 11 shows the distributions of prediction error relative to mass velocity, quality, and length-to-diameter ratio. Due to the lack of CHF data for smaller diameter test sections, the majority of the test data are limited to $L/D_h = 20$–30. The new correlation is valid over the following ranges: $G = 500$ to 2500 kg/m^2.s, $x^*_{e,in} = -1.0$to -0.4, and $P = 1.13$ to 1.48 bar.

3.3. Strategy for exceeding $q''_{eff} = 1000$ W/cm^2

The ability to dissipate 1000 W/cm^2 is a major challenge for advanced defense electronics for which the present study is intended. Ironically, efforts to experimentally demonstrate such

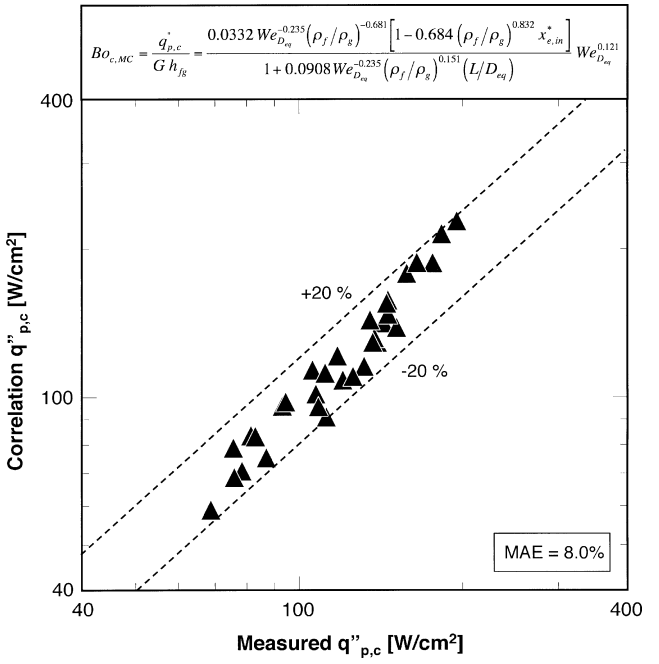

Fig. 10. Comparison of predictions of subcooled boiling CHF correlation and experimental data.

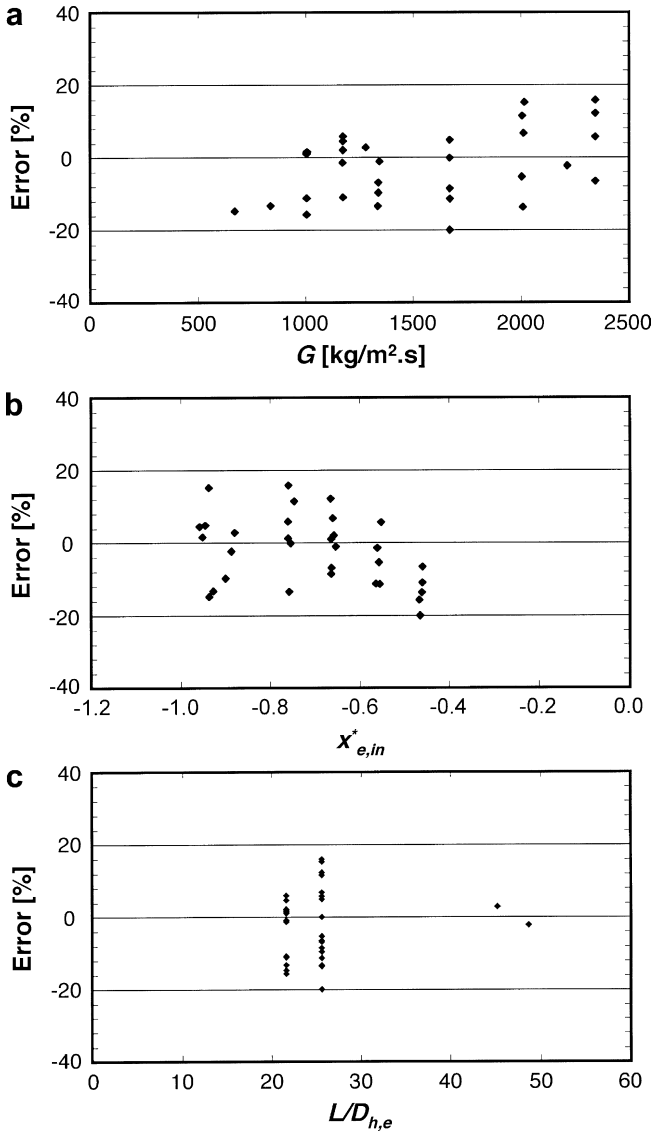

Fig. 11. Error distributions in predictions of subcooled CHF correlation relative to (a) mass velocity, (b) inlet quality, and (c) length-to-hydraulic-diameter ratio.

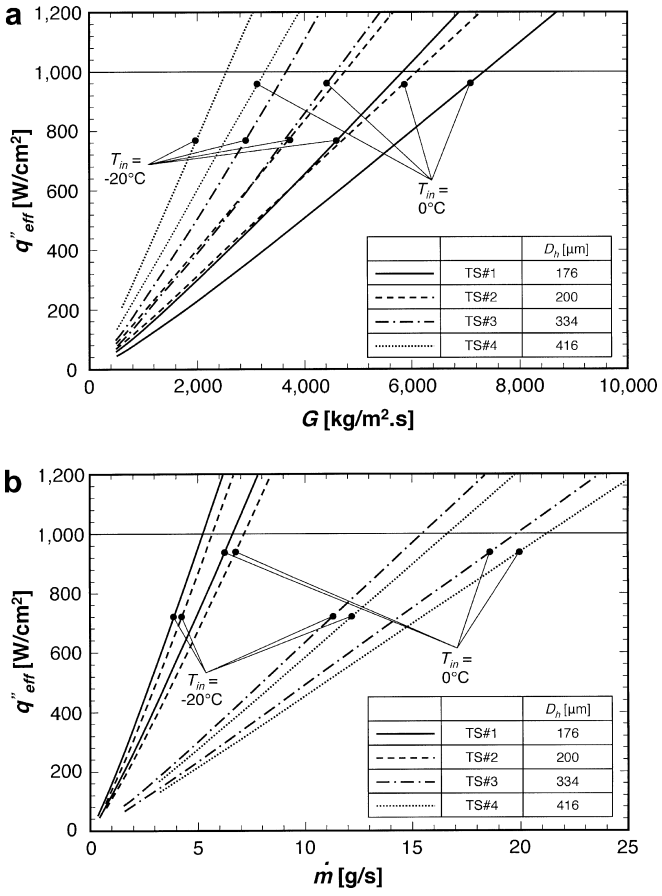

Fig. 12. Conditions required to exceed 1000 W/cm^2: (a) CHF versus mass velocity; (b) CHF versus mass flow rate.

heat dissipation is limited by the ability to construct test heaters that can endure these extreme heating conditions. Large temperature gradients between the cartridge heaters embedded in the test heater and the test surface often produce temperatures that are too high for the materials comprising the test heater, such as plastics and sealants. In the present study, tests had to terminated at about 700 W/cm^2 to avoid damaging the test module parts.

However, using the new CHF correlation, it is possible to determine operating conditions that can yield the required 1000 W/cm^2 heat dissipation. Calculations are based on the four different micro-channel geometries examined in the preset study and two inlet qualities, $x_{in} = -0.65$ (for $T_{in} = 0\ ^\circ C$) and $x_{in} = -0.85$ (for $T_{in} = -20\ ^\circ C$). Outlet pressure is fixed at $P_o = 1.14$ bar.

Fig. 12 shows conditions exist that can easily exceed 1000 W/cm^2. Results are based on G in Fig. 12(a) and $\dot{m}$ in Fig. 12(b); the later provides a more realistic comparison of different micro-channel sizes. Because of their relatively smaller heat transfer area, smaller diameter channels require higher mass fluxes to achieve 1000 W/cm^2 than larger channels. However, on a heat sink basis, smaller diameters can actually exceed 1000 W/cm^2 at lower total coolant flow rates than larger diameters. Decreasing the coolant's inlet temperature (i.e., increasing $\Delta T_{sub,in}$) also decreases the total flow rate required to exceed this heat flux.

Interestingly, the required coolant flow rates according to Fig. 12 are quite feasible with the present indirect refrigeration system. However, aside from the aforementioned high temperatures and test module's material concerns, such flow rates were not possible for the smaller test sections because high pressure drop exceeded the capability of the primary coolant's pump. These findings provide important quantitative practical guidelines for the attainment of the thermal goal.

4. Conclusions

This study explored the critical heat flux (CHF) limit for micro-channel sinks under subcooled flow conditions using HFE 7100 as working fluid. The subcooling was achieved by pre-cooling the fluid using a low-temperature refrigeration system. Prior CHF correlations were modified to accommodate the unique features of micro-channel heat sinks, such as rectangular geometry, three-sided heating and flow interactions between micro-channels. Key conclusions from the study are as follows:

(1) High inlet subcooling greatly reduces both bubble departure diameter and void fraction, precluding any flow pattern transitions beyond the bubbly regime. CHF is triggered by vapor blanket formation along the micro-channel walls despite the abundance of core liquid. This behavior is consistent with the mechanism of Departure from Nucleate Boiling (DNB).

(2) CHF increases with increases in mass velocity and/or subcooling. CHF also increases with decreasing hydraulic diameter for a given total coolant mass flow rate because of the increased mass velocity. Exceptions to the diameter trend are very small diameters and/or very small micro-channel widths that may promote early transition to slug flow.
(3) Weak momentum of incoming liquid at low mass velocities and small inlet subcoolings trigger a pre-mature form of CHF caused by vapor backflow into the inlet. This type of CHF is associated with significant fluctuations in inlet and outlet pressure, as well as wall temperature.
(4) A systematic technique was developed to modify existing CHF correlations to more accurately account for the unique features of micro-channel heat sinks, including rectangular cross-section, three-sided heating, and flow interaction between micro-channels. This technique is successful at correlating the present data for different hydraulic diameters, mass velocities and inlet subcoolings.

Acknowledgement

The authors are grateful for the support of the Office of Naval Research (ONR) for this study.

References

[1] I. Mudawar, Assessment of high-heat-flux thermal management schemes, IEEE Trans. CPMT: Compon. Packaging Technol. 24 (2001) 122–141.
[2] J. Lee, I. Mudawar, Fluid flow and heat transfer characteristics of low temperature two-phase micro-channel heat sinks – Part 1: Experimental methods and flow visualization results, Int. J. Heat Mass Transfer 51 (2008) 4315–4326.
[3] J. Lee, I. Mudawar, Fluid flow and heat transfer characteristics of low temperature two-phase micro-channel heat sinks–Part 2: Subcooled boiling pressure drop and heat transfer, Int. J. Heat Mass Transfer 51 (2008) 4327–4341.
[4] I. Mudawar, M.B. Bowers, Ultra-high heat flux (CHF) for subcooled water flow boiling-I: CHF data and parametric effects for small diameter tubes, Int. J. Heat Mass Transfer 42 (1999) 1405–1428.
[5] D. Hall, I. Mudawar, Ultra-high heat flux (CHF) for subcooled water flow boiling-II: high-CHF database and design equations, Int. J. Heat Mass Transfer 42 (1999) 1429–1456.
[6] D. Hall, I. Mudawar, Critical heat flux (CHF) for water flow in tubes-I. Compilation and assessment of world CHF data, Int. J. Heat Mass Transfer 43 (2000) 2573–2604.
[7] D. Hall, I. Mudawar, Critical heat flux (CHF) for water flow in tubes-II. Subcooled CHF correlations, Int. J. Heat Mass Transfer 43 (2000) 2605–2640.
[8] Y. Katto, A generalized correlation of critical heat flux for the forced convection boiling in vertical uniformly heated round tubes, Int. J. Heat Mass Transfer 21 (1978) 1527–1542.
[9] Y. Katto, General features of CHF of forced convection boiling in uniformly heated rectangular channels, Int. J. Heat Mass Transfer 24 (1981) 1413–1419.
[10] Y. Katto, H. Ohno, An improved version of the generalized correlation of critical heat flux for the forced convective boiling in uniformly heated vertical tubes, Int. J. Heat Mass Transfer 27 (1984) 1641–1648.
[11] M. Kureta, H. Akimoto, Critical heat flux correlation for subcooled boiling flow in narrow channels, Int. J. Heat Mass Transfer 45 (2002) 4107–4115.
[12] C.H. Lee, I. Mudawar, A mechanistic critical heat flux model for subcooled flow boiling based on local bulk flow conditions, Int. J. Multiphase Flow 14 (1988) 711–728.
[13] J. Weisman, B.S. Pei, Prediction of critical heat flux in flow boiling at low qualities, Int. J. Heat Mass Transfer 26 (1983) 1463–1477.
[14] Y.M. Kwon, S.H. Chang, A mechanistic critical heat flux model for wide range of subcooled and low quality flow boiling, Nucl. Eng. Design 188 (1999) 27–47.
[15] W. Qu, I. Mudawar, Measurement and correlation of critical heat flux in two-phase micro-channel heat sinks, Int. J. Heat Mass Transfer 47 (2004) 2045–2059.
[16] L. Wojtan, R. Revellin, J. Thome, Investigation of saturated critical heat flux in a single uniformly heated micro-channel, Exp. Thermal Fluid Sci. 30 (2006) 765–774.
[17] J.R. Thome, Boiling in microchannels: a review of experiment and theory, Heat Fluid Flow 25 (2004) 128–139.
[18] P.A. Kew, K. Cornwell, Correlations for the prediction of boiling heat transfer in small-diameter channels, App. Thermal Eng. 17 (1997).
[19] S.-J. Liao, An analytic approximation of the drag coefficient for the viscous flow past a sphere, Int. J. Non-Linear Mech. 37 (2002) 1–18.
[20] F.P. Incropera, D.P. Dewitt, Fundamentals of heat and mass transfer, Fifth ed., Wiley, New York, 2002.
[21] R.K. Shah, A.L. London, Laminar flow forced convection in Ducts: a source book for compact heat exchanger analytical data, Advances in Heat Transfer Supplement 1, Academic Press, New York, 1978.